

Characterizing the dynamics of rubella relative to measles: the role of stochasticity

Ganna Rozhnova^{*1,2}, C. Jessica E. Metcalf³, and Bryan T. Grenfell^{4,5}

¹Theoretical Physics Division, School of Physics and Astronomy, University of Manchester, Manchester M13 9PL, United Kingdom

²Centro de Física da Matéria Condensada and Departamento de Física, Faculdade de Ciências da Universidade de Lisboa, P-1649-003 Lisboa Codex, Portugal

³Department of Zoology, Oxford University, Oxford, UK

⁴Department of Ecology and Evolutionary Biology, Eno Hall, Princeton University, Princeton, USA

⁵Fogarty International Center, National Institute of Health, Bethesda, Maryland, USA

Abstract

Rubella is a completely immunizing and mild infection in children. Understanding its behavior is of considerable applied importance because of Congenital Rubella Syndrome, which results from infection with rubella during early pregnancy and may entail a variety of birth defects. The dynamics of rubella are relatively poorly resolved, and appear to show considerable diversity globally. Here, we investigate the behavior of a stochastic seasonally forced susceptible-infected-recovered model to characterize the determinants of these dynamics and illustrate patterns by comparison with measles. We perform a systematic analysis of spectra of stochastic fluctuations around stable attractors of the corresponding deterministic model and compare them with spectra from full stochastic simulations in large populations. This approach allows us to quantify the effects of demographic stochasticity and to give a coherent picture of measles and rubella dynamics, explaining essential differences in the patterns exhibited by these diseases. We discuss the implications of our findings in the con-

text of vaccination and changing birth rates as well as the persistence of these two childhood infections.

1 Introduction

Rubella is a completely immunizing, directly transmitted infection, generally expressed as a mild, and potentially even asymptomatic childhood disease [7]. As a result, rubella tends to be under-reported, and its dynamics are fairly poorly characterized. Nevertheless, since infection during early pregnancy may cause spontaneous abortion or Congenital Rubella Syndrome (CRS), which may entail a variety of birth defects [13], understanding the dynamics of rubella is of considerable applied importance. Dynamical features of rubella may alter the CRS burden via their effects on the average age of infection. Episodic dynamics may increase the average age of infection, as the intervals between larger outbreaks provide the opportunity for individuals to age into later age classes [20, 53]. Likewise, local extinction dynamics can allow individuals to remain susceptible as they age into their childbearing years [37, 36], resulting in the potential for a considerable CRS burden once rubella is

*corresponding author: ganna.rozhnova@manchester.ac.uk

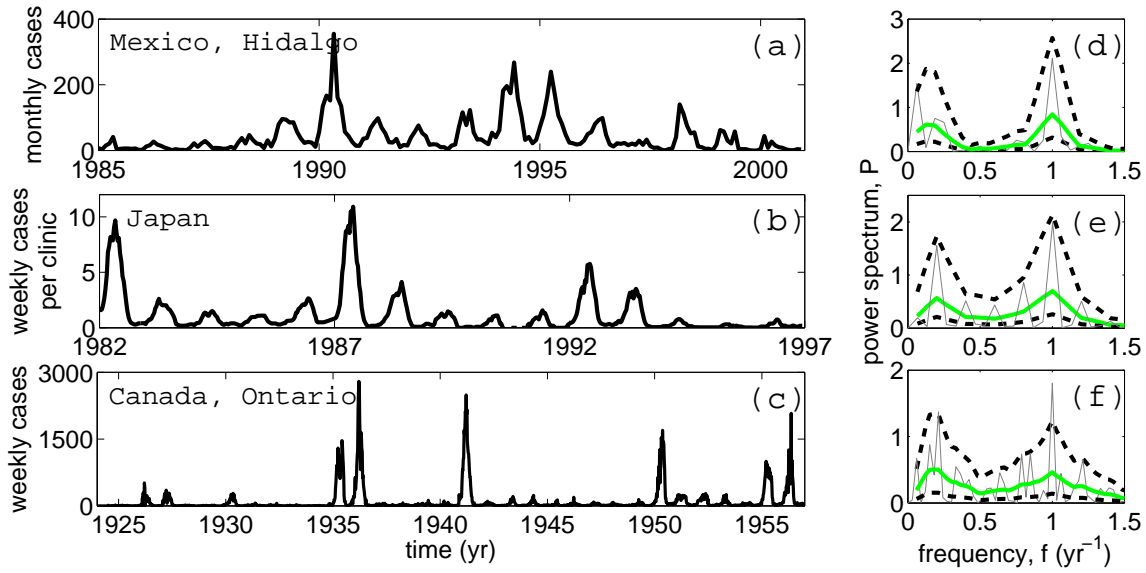


Figure 1: (Color online) Time series of the case reports of rubella and the corresponding spectrum in (a), (d) the Hidalgo district, Mexico; (b), (e) Japan and (c), (f) the province Ontario, Canada. To resolve low-frequency periodicities these time series include short intervals of vaccination (years 1998-2000 for Mexico and 1989-1992 for Japan). Before the spectrum was taken, each series was normalized, setting the mean to zero and the variance to unity. The smooth spectrum (thick green lines) was obtained from the raw spectrum (thin gray lines) using two passes of a 3-point moving average of the spectral ordinates. The dashed black lines are 90% confidence limits on the smooth spectrum. The method of computation of the spectra and confidence limits is described in detail in Chapter 4 of Ref. [15].

re-introduced.

Empirically, rubella seems to be linked to either i) annual dynamics, as in Mexico [35], Peru [35], or parts of Africa [26]; ii) spiky dynamics, as in Canada [6] and iii) some hint at multi-annual regularity, as in Japan [51], England and Wales [4], and various European countries [18], see typical time series in Figure 1. Spectral analysis of time series is particularly useful for understanding temporal patterns exhibited by different data [41, 15]. The characteristic feature of rubella spectra are an annual peak at 1 year and a multi-annual peak at 5-6 years exhibited by all data in Figure 1. Rubella also seems to experience regular fade-outs [35], which is of great epidemiological importance, particularly in the context of increasing global control efforts. The propensity for stochastic extinction is characterised by the critical community size (CCS), below which the infection tends to go extinct in epidemic troughs. Analyses of dynamics in Mexico and Peru suggest a CCS of over 10^6 for rubella [35, 37], as compared to the estimated value of $2.5 \times 10^5 - 3 \times 10^5$ for measles in England and Wales [5].

The two key ingredients underlying models of childhood diseases like rubella and measles are i) seasonality in transmission due to schooling patterns and ii) demographic stochasticity due to the discrete nature of population [47, 16, 28, 40]. Although various approaches have been used to understand the dynamics of rubella [30, 6, 3, 14], most of the analysis has been essentially deterministic. Keeling et. al. [30] considered a term-time forced susceptible-infected-recovered (SIR) model and compared its dynamics to rubella data in Copenhagen. From this, they concluded that the dynamics of rubella may result from switching between two cyclic attractors (annual and multi-annual limit cycles) of the deterministic model. Although the deterministic analysis they present is comprehensive, there is only a limited amount of evidence to suggest that the switching will occur in contexts that include demographic stochasticity. In particular, in this work [30] stochasticity was introduced into the model as multiplicative noise of arbitrary amplitude instead of using, for instance, standard stochastic simulations based on the Gillespie algorithm [25]. Such simulations produce

the exact dynamics of the system subject to demographic stochasticity, which for large populations is described by the deterministic model with additive noise [44, 9].

Bauch et. al. [6] studied a term-time forced susceptible-exposed-infected-recovered (SEIR) model and showed that frequencies obtained from the linear perturbation analysis of the deterministic model are in good agreement with positions of the peaks in spectra of data records of various childhood infections. The application of this approach to rubella data for Canada predicted two distinct peaks at 1 and 5.1 years, close to what we see in Figure 1 (f). To date, there has been little work overall on a fully stochastic approach dealing with demographic stochasticity.

Here, we use this approach to characterize different rubella dynamics and illustrate patterns by comparison with measles. To this end, we perform the theoretical analysis of spectra of stochastic fluctuations around stable attractors of a seasonally forced deterministic SIR model and compare them with spectra obtained from full stochastic simulations based on a modification [2] of the algorithm by Gillespie [25]. The mathematical techniques employed in this work have been developed for ecological and epidemiological models [34, 44, 46] and applied to model temporal patterns of measles and pertussis [45, 9, 10]. The picture that emerges to explain rubella dynamics is close to that proposed in [6] but goes beyond it because our analysis allows us to obtain the full structure of a spectrum (as opposed to the deterministic analysis of [6] where only frequencies of the spectral peaks could be predicted). By introducing key spectral characteristics we systematically investigate how the dominant period, amplitude and coherence of stochastic fluctuations change across a broad range of epidemiological parameters. We then discuss the implications of our analysis in the context of changing birth rates and vaccination levels, as well as their implications for the persistence of measles and rubella.

2 Methods

2.1 Model

The individual-based stochastic model we explore in this paper follows a standard seasonally forced SIR structure [29, 4]. At any time t , it consists of a discrete population of constant size N divided into compartments of susceptible, $S(t)$, infected, $I(t)$, and recovered, $R(t)$, individuals. Susceptible individuals become infected (and infectious) at a frequency dependent rate $\beta(t)I(t)/N$, where $\beta(t)$ is a seasonally varying transmission rate. For childhood diseases, $\beta(t)$ captures an increase in the number of contacts between school children during terms with respect to holidays [47]. We consider a sinusoidally forced $\beta(t) = \beta_0(1 + \epsilon \cos 2\pi t)$, where β_0 is the average transmission rate and ϵ is the amplitude of seasonal forcing. Infected individuals recover at constant rate ν ($1/\nu$ is the average infectious period). As is common in the mathematical epidemiology literature [29, 4], we restrict our attention to the case when birth and death rates μ ($1/\mu$ is the average life-time) are equal, and thus the total population size N is constant. This allows us to reduce the number of independent variables to two and define the state of the system as $\sigma = \{S(t), I(t)\}$. From β_0 , ν and μ we can express one of the most important epidemiological parameters [29, 4], the basic reproductive ratio $R_0 = \beta_0/(\nu + \mu)$. R_0 is the average number of secondary cases caused by one infectious introduced into a fully susceptible population; R_0 will be used throughout the text.

2.2 Theoretical Analysis

Two main approaches can be used to investigate the dynamics of the stochastic model formulated above. An analytical approach starts from the formulation of the model as a master equation for the probability of finding the system in state σ with $S(t)$ susceptibles and $I(t)$ infectives at time t [54, 42, 24]. Much understanding about the stochastic dynamics relevant for recurrent epidemics can be gained if this equation is expanded in powers of $1/\sqrt{N}$ [54]. An extensive discussion of this approach has already been given

at length in the literature in the context of epidemic models, and we refer the reader to [1, 9, 44] for formal details. Here we describe only the aspects which are important for this paper. In essence, the method involves the substitutions $S(t) = N\bar{s} + \sqrt{N}x_S(t)$ and $I(t) = N\bar{i} + \sqrt{N}x_I(t)$ in the master equation which can be then expanded to obtain two systems of equations [54]. At the leading order, the expansion gives rise to a set of ordinary differential equations for the *mean* variables, i.e. the fractions (densities) of susceptible and infected individuals, \bar{s} and \bar{i} . These equations are the same as the standard deterministic SIR model with sinusoidal forcing (see e.g. [28]). At next-to-leading order it gives rise to a set of stochastic differential equations for *fluctuations* of susceptible, $x_S(t)$, and infected, $x_I(t)$, individuals about the mean behavior given by the deterministic model [54]. From these equations we are able to analytically calculate power spectra of fluctuations for susceptibles, $P_S(f)$, and infectives, $P_I(f)$, as functions of frequency f . We are interested in the endemic behavior of the model so the spectra correspond to the fluctuations about *stable attractors* of the deterministic model which for $\epsilon = 0$ and $\epsilon > 0$ are the endemic *fixed point* [1] and stable *limit cycles* with a period that is an integer multiple of a year [9, 44], respectively. Further technical details relating to analytical calculations are given in the Supplementary Electronic Material.

In our analysis we will focus on a spectrum $P_I(f)$, which for simplicity will be denoted as $P(f)$, and its three characteristics, namely *dominant period*, *amplification* and *coherence* [1, 50], see Figure 2. We define the dominant period of stochastic fluctuations as inverse frequency of the maximum of the highest stochastic peak. We also compute the total spectral power which equals the area under a power spectrum curve. This quantity defines the ability of the system to sustain oscillations of all frequencies and shall be referred to as the amplification of stochastic fluctuations. Finally, the coherence is defined as the ratio of spectral power lying within 10% from the dominant period and the total spectral power. It serves to measure how well-structured oscillations about the dominant period are.

As a rule, a theoretical spectrum of unforced epidemic models ($\epsilon = 0$) has one peak [1, 45], while

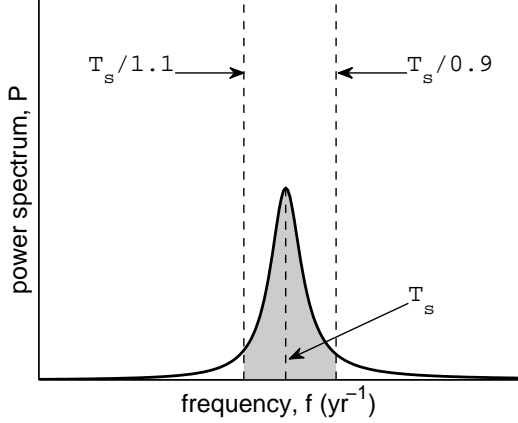


Figure 2: Schematic plot of a power spectrum of stochastic fluctuations for infectives, $P(f)$. The quantities used in the comparative analysis of different spectra are the dominant period (the inverse of the main peak’s frequency), amplification (total area under the power spectrum curve) and coherence (ratio of the shaded area to the total area).

it can have several peaks of different amplitudes for $\epsilon > 0$ [9, 44]. Away from bifurcation points of the deterministic model, one of them is usually much higher than the others. We are not aware of any work assessing the relevance of secondary peaks to recurrent epidemic behavior seen in real data. The highest peak, however, has been shown to be important in understanding the inter-epidemic periods observed in time series of pertussis and measles [9, 10, 45], and is therefore used in the definition of a spectrum’s characteristics in this paper.

2.3 Simulations

We simulate the model using an extension of Gillespie’s algorithm [2, 25] which produces stochastic trajectories for $\{S(t), I(t)\}$ in continuous time. These are processed further to compute numerical spectra and test them against the theoretical prediction for $P(f)$. The simulation length is 500 years and the first 50 years are discarded. In numerical work

a time series for fluctuations $x_I(t)$ is obtained as $x_I(t) = [I(t) - N\bar{i}] / \sqrt{N}$, where \bar{i} is the fraction of infectives averaged over many realizations of the model. From $x_I(t)$ we compute a spectrum $P(f)$ using the discrete Fourier transform. For $\epsilon > 0$ we also present a spectrum of the entire ‘signal’ (scaled by population size N), $I(t)$, which will be referred to as a *full* spectrum. By definition $P(f)$ includes only stochastic peaks, while the full spectrum includes both deterministic peaks corresponding to a limit cycle and stochastic peaks corresponding to fluctuations about it. For each set of parameters, 250 simulations starting from random initial conditions are recorded, and all final spectra are averaged over those where no extinctions occurred during 500 years.

3 Results

We compare the numerical and theoretical predictions for different spectra and the three measures we have conventionally chosen to characterise them. In the beginning we explore a large region of parameter space and later discuss the main findings for rubella and measles.

3.1 No seasonal forcing: $\epsilon = 0$

3.1.1 Theoretical and simulation results

We first restrict our attention to the case when there is no seasonality, for which an explicit expression for the analytical spectrum can be found (see the Supplementary Electronic Material). The deterministic SIR model has only one endemic fixed point provided $R_0 > 1$ [29, 4]. Figure 3 shows analytical and numerical results for the dominant period of stochastic fluctuations about it as well as their amplification and coherence for a range of basic reproductive ratios, R_0 , and infectious periods, $1/\nu$. Analytical spectra can be obtained for any $R_0 > 1$. In practice long numerical simulations may not be feasible for all parameter combinations where $R_0 > 1$ because the system experiences frequent extinctions when the infectious period is short. The results presented in Figure 3 are for a typical population size of a large city, $N = 10^6$, and the domain where this happens is shown in gray.

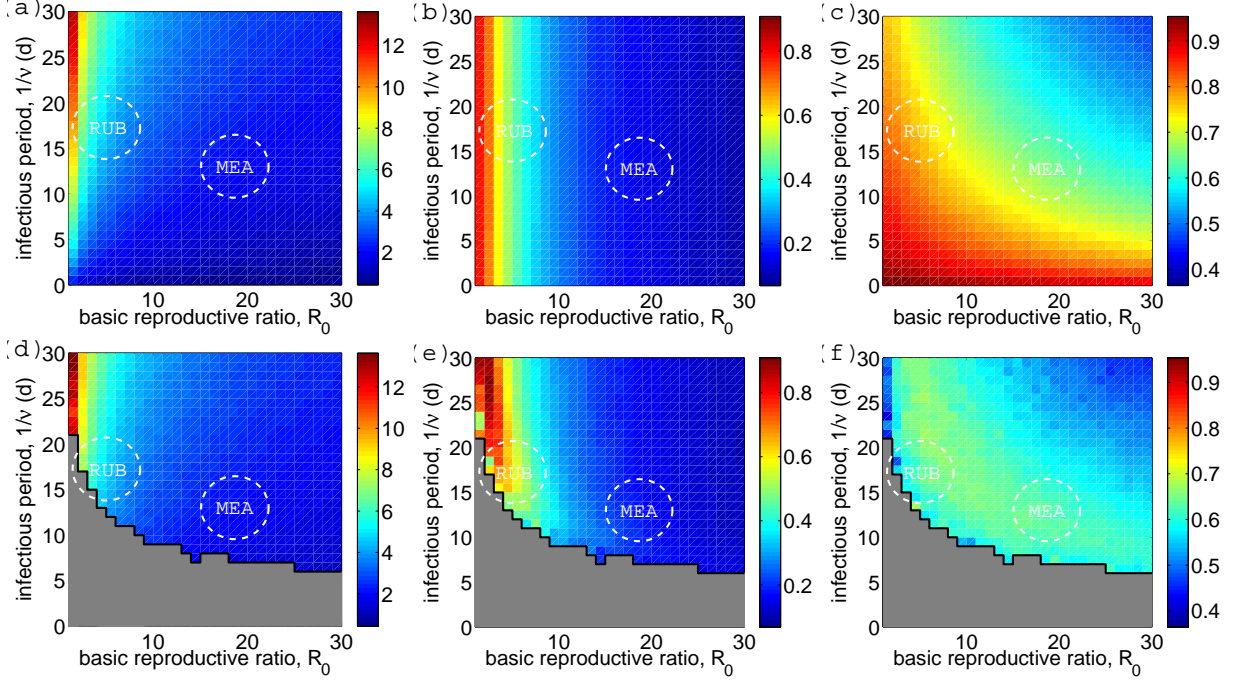


Figure 3: (Color online) Analytical (top) and simulation (bottom) results for the (a), (d) dominant period of stochastic fluctuations about the endemic fixed point, (b), (e) amplification and (c), (f) coherence. The black staircase graph bounds the gray region where all simulations went extinct within 500 years. Approximate parameter values for measles and rubella are depicted as dashed circles. Parameters: $\epsilon = 0$, $\mu = 0.02$ 1/y and $N = 10^6$.

In the region of parameter space amenable to the exploration of the long-term dynamics of the model, we observe that the structure of the spectra uncovered by the theory is clearly visible in the simulations too. Small systematic deviations between the two predictions are expected and occur close to the extinction boundary. These are mainly reflected in the broadening of a spectrum and appearance of secondary peaks. As a consequence, amplification, see Figure 3 (e), is slightly increased (coherence, Figure 3 (f), is correspondingly decreased) in the simulations in the area adjacent to the gray region. In addition to these changes, an increase of the dominant period of stochastic fluctuations in the simulated spectra may be observed [50, 44]. This effect will be discussed in more detail in the next section where seasonality is included, as without seasonality, it is only barely apparent (compare Figure 3 (a) and (d)).

3.1.2 Implications for rubella and measles dynamics

The structure discovered in Figure 3 allows us to derive an initial picture of the dynamics of rubella relative to measles. Based on estimates of parameters typical of these diseases for the pre-vaccination era [4, 30, 28, 6, 8, 35] we superimpose their approximate locations in all panels of Figure 3. The rubella estimates are for Mexico and Canada, and the measles estimates are for England and Wales. For rubella the infectious period, $1/\nu$, is about 18 days and R_0 ranges from 3.4 to 9.5 in Mexico, in particular it was estimated to be 5.3 to 6.7 in the Mexico's district Hidalgo (Figure 1 (a)). R_0 in the Canadian province Ontario ranges from 4.6 to 6.5 where the upper bound is the estimate for the years shown in Figure 1 (c). For measles we have taken the most frequently used values for large cities (e.g. London) in England and Wales before vaccination, $1/\nu$ about 2 weeks and R_0 around 18.

The results so far ignore the seasonality of transmission rate and so are insufficient to explain the patterns of measles in which it plays a pivotal role [8, 19, 28]. However, they have important implications for understanding the dynamics of rubella. As we shall confirm shortly, for $\epsilon > 0$ the spectrum

of stochastic fluctuations for this disease is close in form to that obtained for the unforced model which correctly predicts a dominant period of about 5-6 years (Figure 3 (a) and (d)) as seen in the data (Figure 1). This period is similar to the natural period of small amplitude perturbations from the endemic fixed point recovered in the purely deterministic setting [30].

Our analysis of the stochastic model allows us to quantify other features of fluctuations using amplification and coherence, see Figure 3 (b)-(c) and (e)-(f). For rubella, the amplification is large indicating that the epidemic patterns of the unforced model represent high amplitude oscillations. High coherence suggests that only a few of the frequencies involved in the stochastic fluctuations account for most of the variance of time series. This peculiar type of dynamics sets rubella close to the extinction boundary. Large coherent multi-annual epidemics with troughs deeper than in the region with higher R_0 cause regular fade outs. In the next section, we discuss how these descriptions of the stochastic dynamics of rubella are changed in the presence of seasonality and compare it with the dynamics of measles.

3.2 Seasonal forcing: $\epsilon > 0$

3.2.1 Theoretical and simulation results

For $\epsilon > 0$ the spectra are associated with stochastic fluctuations about stable attractors of the deterministic model, i.e. stable limit cycles of a period in multiples of a year [44, 9]. The seasonally forced deterministic SIR model has a complex bifurcation diagram with regimes where multiple limit cycles may coexist [31, 52]. For high birth rates and high seasonality regions corresponding to chaotic dynamics are found [21]. Across most of the range of parameter space we explore here, either annual or biennial limit cycles are present. We performed the theoretical analysis for these attractors for different parameters and found that the agreement between the theory and simulations is in general excellent. Nevertheless, small discrepancies are again expected if a limit cycle is not sufficiently stable and/or a population is small. In particular, this happens near the extinc-

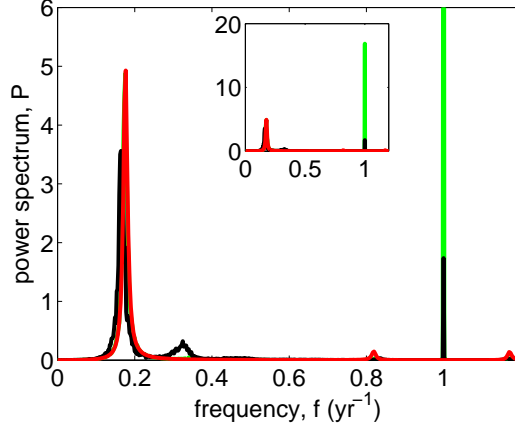


Figure 4: (Color online) Analytical spectra of stochastic fluctuations around an annual cycle (red lines) and full numerical spectra (black and green lines) for the seasonally forced model. The red line is indistinguishable from the green line except for in the vicinity of 1 year. For clarity in the comparison one of the peaks at 1 year is cropped in the main panel while the entire spectra can be seen in the inset. Parameters: $\epsilon = 0.05$, $\mu = 0.02$ 1/y, $R_0 = 4$, $1/\nu = 18$ d, $N = 10^6$ (black) and $N = 10^7$ (green).

tion boundary, and is therefore relevant for rubella.

For parameters reflecting rubella, an annual limit cycle is found in the deterministic model. To illustrate the effects of population size on simulated spectra we show in Figure 4 an analytical spectrum about this attractor (red line) and full numerical spectra for $N = 10^6$ (black line) and $N = 10^7$ (green line). For the larger population size, the simulated spectrum exhibits two types of peaks. There is a dominant annual peak (corresponding to the deterministic annual cycle) and a subdominant broad multi-annual peak (corresponding to stochastic fluctuations about it). The latter is indistinguishable from the theoretical spectrum (red and green lines coincide except for in the vicinity of 1 year).

The amplitude of the deterministic peak scales with population size and for $N = 10^6$ the peak at 1 year becomes subdominant, see the black line in Figure 4. This indicates that the contribution of an annual component in the time series decreases with decreasing N . As for fluctuations beyond the annual component, at least two stochastic peaks at 5.8 and 2.9 years can be clearly seen. Although the theory does not capture them in full, the agreement is still

good and, more importantly, the systematic qualitative changes can be predicted. For small populations, the dominant period of fluctuations in simulations is slightly increased and their variance is distributed over a larger range of frequencies with respect to theoretical predictions [44]. This is compatible with a general observation of the increased stochasticity and therefore much more irregular dynamics in small populations [27, 32]. The example we presented here was for $R_0 = 4$, which neighbors the extinction boundary. Simulations for larger R_0 show smaller deviations from analytical calculations even for populations as small as $N = 10^6$.

Another situation which the analytical theory cannot fully account for is stochastic switching between different attractors of the deterministic model [17, 30]. The computation of an analytical spectrum about a limit cycle requires the knowledge of its geometric orbit (see Supplementary Electronic Material). In the sinusoidally forced SIR model several stable attractors coexist in the regions of small R_0 and $1/\nu$ [31] and spectra of stochastic fluctuations about each of them can be obtained separately [44]. The theoretical analysis, however, does not allow us

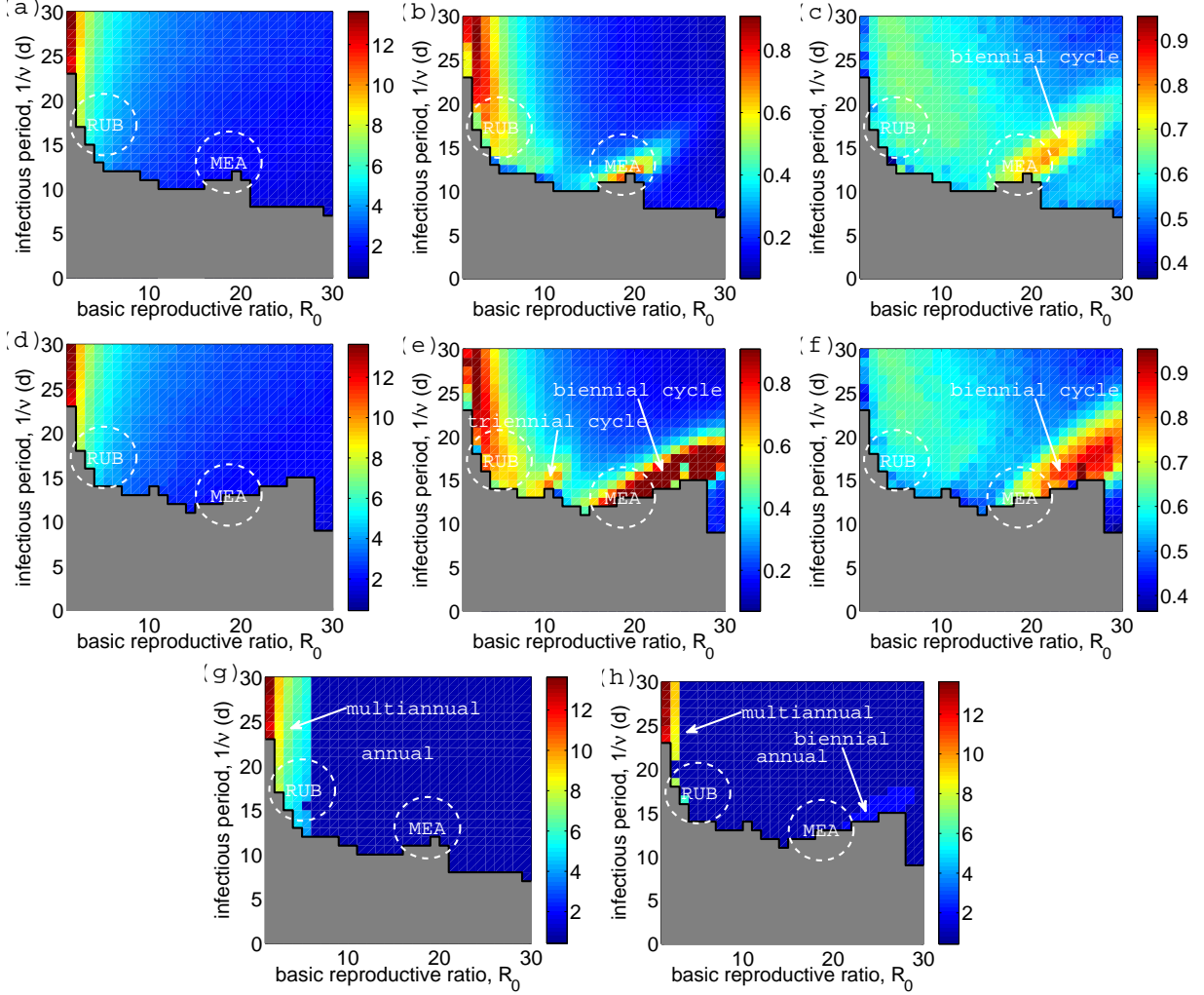


Figure 5: (Color online) Simulation results for the (a), (d) dominant period of stochastic fluctuations, (b), (e) amplification, (c), (f) coherence and (g), (h) dominant period in the full spectrum. The seasonality is twice larger in the second row and panel (h) than in the first row and panel (g). The black staircase graph bounds the gray region where all simulations went extinction within 500 years. Approximate parameter values for measles and rubella are depicted as dashed circles. Parameters: $\mu = 0.02$ 1/y, $N = 10^6$, (a)-(c) and (g) $\epsilon = 0.05$, (d)-(f) and (h) $\epsilon = 0.1$.

to predict which of the attractors will be observed in simulations and what their relative contribution to the total stochastic dynamics is. Previous analysis of the stochastic dynamics of measles and pertussis showed that the only attractors seen in simulations of the seasonally forced SIR model (and other related models of infectious diseases) are annual and biennial cycles [44, 9, 45]. The stochastic switching was observed to happen exclusively between these attractors and only for measles. This result is, however, of limited value to us because it is restricted to particular parameter choices, and so we cannot assume that the switching does not happen in the broader span of the parameter space.

Spectra from simulations contain complete information about the frequency distribution of oscillations and are thus helpful to identify switching between attractors through the presence of unexpected peaks. Figure 5 shows simulation results for the dominant period of stochastic fluctuations, amplification and coherence for two values of seasonality ϵ and $N = 10^6$. In addition to these quantities we compute the dominant period in the full spectrum which includes both stochastic and deterministic peaks.

To examine the effect of seasonality on stochastic fluctuations Figure 5 (a)-(f) can be directly compared with Figure 3 (a)-(f) for the unforced model. As ϵ increases the (gray) domain with frequent extinctions is extended and approaches the measles parameters. For most values of R_0 and $1/\nu$ we have explored (the colored region) the dynamics of the stochastic model are associated with fluctuations about only few attractors. Firstly, the biennial cycle is found inside the region of increased coherence and amplification in Figure 5 (b)-(c) and (e)-(f) which includes measles and is absent in Figure 3 (b)-(c) and (e)-(f). The dominant period in the full spectrum of time series demonstrating such a behavior is at 2 years (Figure 5 (h)). Secondly, stochastic switching between annual and triennial cycles is detected in a small region relevant for measles with low values of R_0 , see an unexpected increase of amplification in Figure 5 (e) around $R_0 = 10$. The spectra here have a dominant annual peak (Figure 5 (h)) and a subdominant triennial peak (Figure 5(d)). The amplification of oscillations associated with the latter is however much

higher than what we would expect to see for fluctuations around an annual cycle (see, e.g. Figure 5 (b)). Thirdly, in the rest of the (colored) region which includes rubella, the spectra are similar to those of the unforced model. The dynamics of the stochastic model here corresponds to fluctuations about an annual cycle and we discuss it first.

3.2.2 Implications for rubella and measles dynamics

From Figure 5 (a) and (d) we see that for relatively small basic reproductive ratios, typical of rubella, the seasonality does not affect the dominant period of stochastic fluctuations which continues to be centered at about 5-6 years. The amplification (coherence) is only slightly increased (decreased) as ϵ increases (Figure 5 (b)-(c) and (e)-(f)). The full spectra of rubella resemble that of Figure 3 with a sharp peak at 1 year and a broad multi-annual peak.

For future discussion of the implications of vaccination and decline or increase in birth rates, it is useful to investigate how the spectra of rubella change with R_0 . Keeping the amplitude of seasonal forcing and infectious period of rubella fixed and increasing R_0 , we expect the period of stochastic fluctuations as well as their amplification to decrease. This is seen from Figure 5 and also illustrated in Figure 6 (a) where the full spectra for parameters close to rubella estimates are shown. The relative contribution of multi-annual and annual frequency components in model time series can be read from the same figure. For small R_0 the fluctuations are large and the multi-annual peak is dominant but for larger R_0 it becomes subdominant and the annual peak is enhanced. The increase of ϵ (or of population size as discussed before) results in the enhancement of the deterministic peak too (compare Figure 5 (g) and (h)), but does not change the dominant period of fluctuations significantly.

For measles, there are major changes in the behavior as both coherence and amplification increase drastically for $\epsilon > 0$, see the newly appeared oval-shaped regions near measles parameters in Figure 5 (b)-(c) and (e)-(f). To demonstrate that this phenomenon indicates the appearance of a biennial cycle

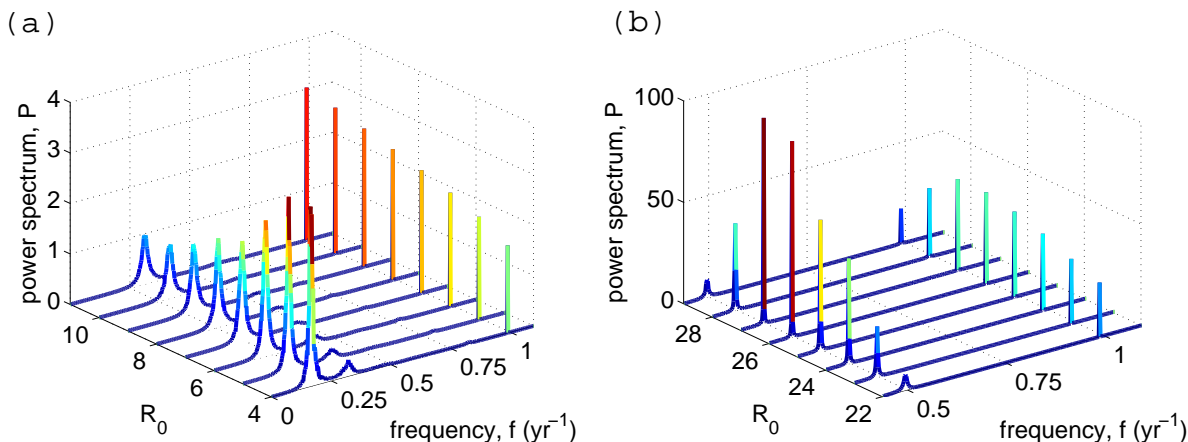


Figure 6: (Color online) Full spectra from simulated time series, corresponding to the dynamics typical of (a) rubella and (b) measles. The color intensity increases (from blue to red) with increasing power. Parameters: $\mu = 0.02$ 1/y, $N = 10^6$, (a) $\epsilon = 0.05$, $1/\nu = 18$ d, (b) $\epsilon = 0.1$, $1/\nu = 16$ d.

in simulations we show in Figure 6 (b) the full spectra for fixed infectious period, $1/\nu = 16$ d, and a range of $R_0 \in [22, 29]$. These values of $1/\nu$ and R_0 are slightly higher than the commonly used estimates for measles in England and Wales, e.g. $1/\nu = 13$ d and $R_0 = 18$ for London before vaccination. The same qualitative dynamics is observed for lower values if the simulation length is shorter than 500 years (results not shown). For $R_0 = 22$ the spectra are typical of fluctuations about an annual limit cycle with a deterministic peak at 1 year and a broad stochastic peak near 2 years. If R_0 is increased further the fluctuations around an annual cycle become macroscopic (the stochastic peak at 2 years becomes much higher) smoothly turning into a biennial limit cycle. This transition corresponds to a period doubling bifurcation in the deterministic model. A strong biennial behavior with a dominant peak at 2 years and a secondary harmonic at 1 year is observed for example, for $R_0 = 26$. Finally, for even larger R_0 we see a transition from biennial to an annual cycle again. The set of transitions seen in Figure 6 (b) is typical of measles and have been observed in related models of infections dynamics via analytical and numerical studies by other researches [49, 48, 17, 9, 44, 52].

The seasonality would act to change the picture in

Figure 6 (b) in the following way. From the comparison of Figure 5 (g) and (h) the region of parameter space where such a behavior is seen is expected to get larger with increasing ϵ , in particular for $\epsilon > 0.1$ the period doubling transition is induced for values of R_0 much smaller than in Figure 6 (b).

Previous analysis of measles data from England and Wales and the USA has shown that transitions in the dynamics due to an increase or decline of birth rates as well as the introduction of vaccination are associated with transition between annual and biennial limit cycles [17]. Using a simple mapping from changes in vaccination and birth rates to effective changes in R_0 introduced in [17], our results confirm this view. For large communities with very high birth rates (high R_0) such as Liverpool before vaccination, US cities in the period after the Great Depression or cities in developing countries, we would expect to be in the regime with an annual cycle [22, 23, 17, 11]. Other large cities with smaller birth rates such as London are in the regime with a biennial cycle [28]. The corresponding spectrum with narrow and sharp peaks at 2 and 1 years has been the main reason of more regular and thus more predictable patterns of measles epidemics in large cities. The vaccination introduced in UK in 1968 lowered R_0 and induced a

transition from the biennial to the annual cycle with large stochastic fluctuations. Our analysis thus offers an insight into the factors responsible for the shift from regular epidemics of measles before vaccination to less irregular in the vaccine era [43].

The last finding deserving a further comment concerns the switching between an annual and triennial cycles found for moderate values of R_0 , see Figure 5 (e). This behavior may be responsible for the triennial cycles observed in Baltimore and other US cities during the Great Depression [33] but more thorough analysis is needed to confirm this.

4 Discussion

In this paper, we have investigated the behavior of the stochastic seasonally forced SIR model based on spectra of long time series for a large range of basic reproductive ratios and infectious periods. For relatively low values of R_0 relevant for rubella the model predicts spectra with a stochastic multi-annual peak at about 5-6 years and a deterministic annual peak. Both peaks are observed in the spectra of rubella data (Figure 1). The multi-annual peak stays largely unchanged under the introduction of seasonality (Figures 3 and 5 (a), (d)) or population size (Figure 4) which explains its presence in time series from different locations.

A visual inspection of simulated time series demonstrates intriguing behavior emerging from the interaction between stochasticity and a deterministic annual cycle. Figure 7 shows typical time series for the unforced (red dashed line) and seasonally forced (blue solid line) cases. If $\epsilon = 0$ the epidemic patterns represent multi-annual coherent oscillations. As ϵ is increased we find qualitatively different dynamics all of which correspond to spectra with a multi-annual and an annual peak. Figure 7 (a) shows an example of annual epidemics of alternating amplitudes modulated by an oscillation of a long period corresponding to the period of stochastic multi-annual fluctuations. This dynamic is qualitatively similar to the multi-annual regularity observed, for example, for rubella in Japan (Figure 1). We also find very large outbreaks followed by outbreaks of much lower amplitude as in Figure 7

(b). Such a behavior may be responsible for the spiky dynamics observed in, for example, Canada (Figure 1). Note that the spikes in the data could also arise from spatial effects such as local extinction of the disease followed by reintroduction from another region. However, as we do not possess more resolved data it is impossible to reach a final conclusion with regards to this issue.

The patterns of rubella incidence in large populations are in contrast with those of measles. For the latter the spectra are characterised by sharp and narrow peaks at 1 and 2 years (as opposed to the broad multi-annual peak and a narrow peak at 1 year observed for rubella) and thus correspond to much more regular dynamics. The transitions in measles behavior due to vaccination or change in birth rates are associated with transitions between the annual and biennial limit cycles of the deterministic model. In future work, it would be interesting to study stochastic measles dynamics for higher levels of seasonal forcing that correspond to chaos in the deterministic model [21].

Both measles and rubella are found to be close to the extinction boundary, and increasing the amplitude of seasonal forcing only extends the region of parameter space with frequent fade-outs. Figure 8 illustrates typical stochastic trajectories from simulation in the susceptible-infected plane from which the spectra were computed. Interestingly, these patterns suggest that the mechanism accounting for high extinction probability are different for rubella and measles. For rubella, extinction occurs as a consequence of large stochastic fluctuations about a small (and globally less stable) annual limit cycle, see Figure 8 (a). For measles, extinctions are mainly due to the shape of a large (and globally more stable) biennial limit cycle, from which the system can be driven to extinction by even relatively small fluctuations, see Figure 8 (b).

We can use the framework developed to predict the effect on persistence of an effective reduction in R_0 by vaccination or declining birth rates for rubella and measles. For measles in the biennial regime, either an increase or a decrease of R_0 can lead to fluctuations around an annual cycle (rather than a biennial cycle) that could result in lower extinction rates and

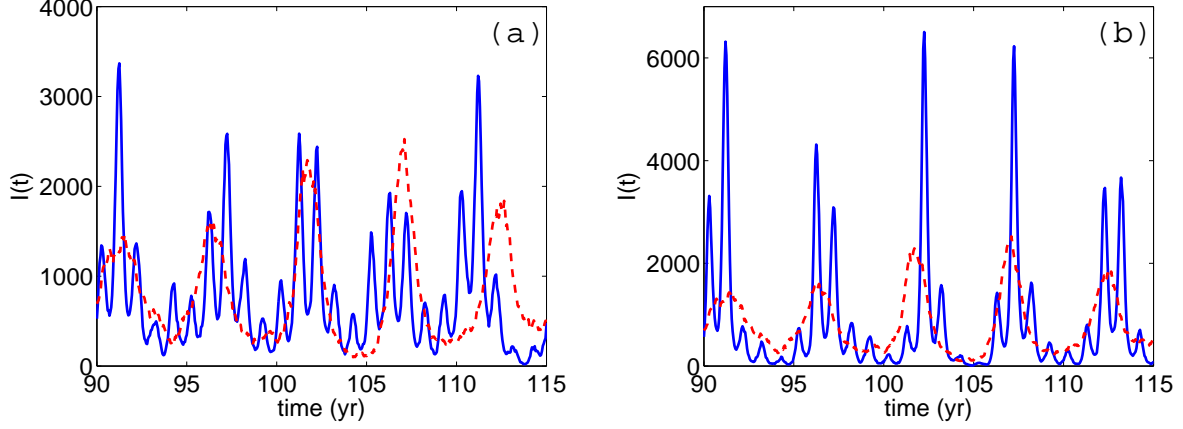


Figure 7: (Color online) Typical time series for rubella parameters. Parameters: $N = 10^6$, $\mu = 0.02$ 1/y, $R_0 = 5$, $1/\nu = 18$ d, $\epsilon = 0$ (dashed red line), (a) $\epsilon = 0.2$ (solid blue line), (b) $\epsilon = 0.3$ (solid blue line).

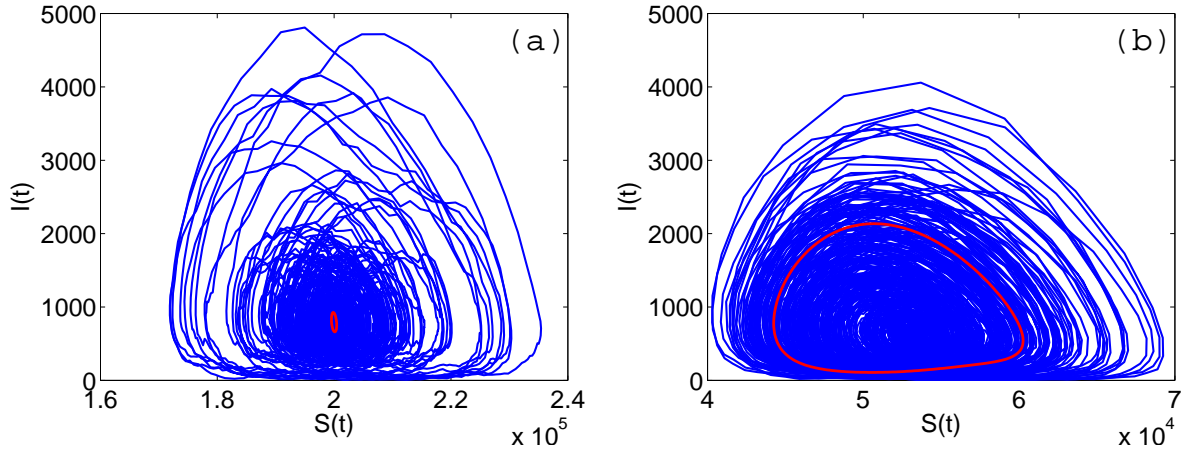


Figure 8: (Color online) Typical stochastic trajectories from simulation (blue solid lines) shown in the susceptible-infected plane. The red line is the deterministic annual cycle in (a) and the biennial cycle in (b). For the parameters used in this figure many simulations go extinct quite fast, for illustration purposes we have chosen the ones which lasted for 500 years. Parameters: $N = 10^6$, $\epsilon = 0.05$, $\mu = 0.02$ 1/y, (a) $R_0 = 5$, $1/\nu = 18$ d (close to rubella estimates), (b) $R_0 = 19$, $1/\nu = 12$ d (close to measles estimates).

thus higher persistence. For rubella, a reduction in R_0 will lead to larger and more coherent oscillations that would unambiguously result in higher extinction probabilities, and thus lower persistence. Both these outcomes merit serious consideration in a public health context: vaccination against measles can make local elimination less likely [21]; while vaccination against rubella is likely to increase local extinction, allowing the buildup of susceptible individuals in later age classes [35, 37], potentially leading to an increase in the burden of Congenital Rubella Syndrome.

These conclusions point to a need for theoretical developments towards uncovering the mechanisms of stochastic extinctions in small population based on the analysis of epidemic models (a thorough overview of studies in this area aiming at understanding the persistence of measles is given in the recent work by Conlan et. al. [12]). In the mathematical framework we adopted in this paper, the approach to computation of the distribution of extinction times in an unforced stochastic epidemic model was proposed some time ago [38, 39]. Nevertheless, no analytical progress can be made along the same lines for the seasonally forced model we use here.

Our focus has been on measles and rubella; however, the broad span of parameter space explored means that our results may shed light on the dynamics of other diseases whose dynamics can be described by a simple SIR formalism with seasonal forcing; for example pertussis [40, 45]. Although the infection with pertussis does not confer permanent immunity the SIR model has been shown to capture the qualitative patterns to some extent [45]. Taking the pertussis parameters before vaccination that are well established in independent data sources (see e.g. [4, 6], $1/\nu = 22$ d and $R_0=17$ for London and Ontario, Canada) from Figure 5 we see that for pertussis the dominant period of stochastic fluctuations is 2 to 3 years. These periods are in the agreement with the documented interepidemic periods [45, 6]. We also find that the coherence of fluctuations is very low, which is compatible with the famously irregular dynamics of pertussis. The decrease of R_0 due to vaccination would act to increase the dominant period and coherence which also agrees with the observation

of the shift to more regular dynamics in the vaccine era [43].

To conclude, in this paper, we used a stochastic framework to explain the dynamics of rubella, particularly in comparison to measles. Our analysis revealed that whilst both rubella and measles are relatively close to their extinction boundary, the reasons for this are very different. Finally, our analysis showed that for rubella, reducing R_0 by vaccinating, or a declining birth rate unambiguously result in higher extinction probabilities, whereas, for measles, outcomes can be more complicated; and both these facts have public health implications.

Acknowledgements

We thank Kihei Terada for helpful discussion of rubella dynamics in Japan; Alan McKane for his careful reading and comments on the paper; and Otmar Bjørnstad for the help with the computation of the confidence intervals for data spectra. Rozhnova gratefully acknowledges the financial support from the Portuguese Foundation for Science and Technology under Contract No. SFRH/BPD/69137/2010. Grenfell was supported by the RAPIDD program of the Science & Technology Directorate, Department of Homeland Security and the Fogarty International Center, National Institutes of Health. Metcalf and Grenfell were supported by the Bill and Melinda Gates Foundation.

References

- [1] D. Alonso, A. J. McKane, and M. Pascual. Stochastic amplification in epidemics. *Journal of the Royal Society Interface*, 4:575–582, 2007.
- [2] D. F. Anderson. A modified next reaction method for simulating chemical systems with time dependent propensities and delays. *Journal of Chemical Physics*, 127:214107, 2007.
- [3] R. M. Anderson and B. T. Grenfell. Quantitative investigations of different vaccination policies for the control of congenital rubella syn-

- drome (CRS) in the United Kingdom. *Journal of Hygiene of Cambridge*, 96:305–333, 1986.
- [4] R. M. Anderson and R. M. May. *Infectious diseases of humans*. Oxford University Press, Oxford, OX2 6PD, 1991.
 - [5] M. S. Bartlett. The critical community size for measles in the United States. *Journal of the Royal Statistical Society, Series A*, 123:37–44, 1960.
 - [6] C. T. Bauch and D. J. D. Earn. Transients and attractors in epidemics. *Proceedings of the Royal Society of London, Series B*, 270:1573–1578, 2003.
 - [7] J. M. Best. Rubella. *Seminars in Fetal and Neonatal Medicine*, 12:182–192, 2007.
 - [8] O. N. Bjørnstad, B. Finkenstädt, and B. T. Grenfell. Endemic and epidemic dynamics of measles: Estimating epidemiological scaling with a time series SIR model. *Ecological Monographs*, 72:169–184, 2002.
 - [9] A. J. Black and A. J. McKane. Stochastic amplification in an epidemic model with seasonal forcing. *Journal of Theoretical Biology*, 267:85–94, 2010.
 - [10] A. J. Black and A. J. McKane. Stochasticity in staged models of epidemics: quantifying the dynamics of whooping cough. *Journal of the Royal Society Interface*, 7:1219–1227, 2010.
 - [11] A. J. K. Conlan and B. T. Grenfell. Seasonality and the persistence and invasion of measles. *Proceedings of the Royal Society of London, Series B*, 274:1133–1141., 2007.
 - [12] A. J. K. Conlan, P. Rohani, A. L. Lloyd, M. J. Keeling, and B. T. Grenfell. Resolving the impact of waiting time distributions on the persistence of measles. *Journal of the Royal Society Interface*, 7:623–640, 2010.
 - [13] L. Z. Cooper and S. Krugman. Clinical manifestations of postnatal congenital rubella. *Archives of Ophthalmology*, 77:434–439, 1967.
 - [14] Th. M. de Boo, J. A. M. van Druten, and A. D. Plantinga. Predicting the dynamic effects of rubella vaccination programmes. *Statistics in medicine*, 6:843–851, 1987.
 - [15] P. J. Diggle. *Time series: a biostatistical introduction*. Clarendon Press, Oxford, 1990.
 - [16] R. Durrett and S. Levin. The importance of being discrete (and spatial). *Theoretical Population Biology*, 46:363–394, 1994.
 - [17] D. J. D. Earn, P. Rohani, B. M. Bolker, and B. T. Grenfell. A simple model for complex dynamical transitions in epidemics. *Nature*, 287:667–670, 2000.
 - [18] W. J. Edmunds, N. J. Gay, M. Kretzschmar, and H. Wachmann. The pre-vaccination epidemiology of measles, mumps and rubella in Europe: implications for modelling studies. *Epidemiology and Infection*, 125:635–650, 2000.
 - [19] M. J. Ferrari, A. Djibo, and R. F. Grais. Rural-urban gradient in seasonal forcing of measles transmission in Niger. *Proceedings of the Royal Society of London, Series B*, 277:2775–2782, 2011.
 - [20] M. J. Ferrari, A. Djibo, R. F. Grais, B. T. Grenfell, and O. N. Bjørnstad. Episodic outbreaks bias estimates of age specific force of infection: a corrected method using measles in Niamey, Niger as an example. *Epidemiology and Infection*, 138:108–116, 2010.
 - [21] M. J. Ferrari, R. F. Grais, N. Bharti, A. J. K. Conlan, O. N. Bjørnstad, L. J. Wolfson, P. J. Guerin, A. Djibo, and B. T. Grenfell. The dynamics of measles in sub-Saharan Africa. *Nature*, 451:679–684, 2008.
 - [22] B. F. Finkenstädt and B. T. Grenfell. Empirical determinants of measles metapopulation dynamics in England and Wales. *Proceedings of the Royal Society, Series B*, 265:211–220, 1998.

- [23] B. F. Finkenstädt and B. T. Grenfell. Time series modelling of childhood diseases: a dynamical systems approach. *Journal of the Royal Statistical Society, Series C*, 49:187–205, 2000.
- [24] C. W. Gardiner. *Handbook of Stochastic Methods*. Springer, Berlin, 2003.
- [25] D. Gillespie. A general method for numerically simulating the stochastic time evolution of coupled chemical reactions. *Journal of Computational Physics*, 22:403–434, 1976.
- [26] J. L. Goodson, B. G. Maresha, A. Dosseh, C. Byabamazima, D. Nshimirimana, S. L. Cochi, and S. Reef. Rubella epidemiology in Africa in the prevaccine era, 2002–2009. *Journal of Infectious Diseases*, 204:S215–S225, 2011.
- [27] B. T. Grenfell, O. N. Bjørnstad, and B. F. Finkenstädt. Endemic and epidemic dynamics of measles: Scaling noise, determinism and predictability with the time series SIR model. *Ecological Monographs*, 72:185–202, 2002.
- [28] M. J. Keeling and B. T. Grenfell. Understanding the persistence of measles: reconciling theory, simulation and observation. *Proceedings of the Royal Society of London, Series B*, 269:335–343, 2002.
- [29] M. J. Keeling and P. Rohani. *Modeling infectious diseases in humans and animals*. Princeton University Press, New Jersey, 08540, 2008.
- [30] M. J. Keeling, P. Rohani, and B. T. Grenfell. Seasonally forced disease dynamics explored as switching between attractors. *Physica D*, 148:317–335, 2001.
- [31] Y. A. Kuznetsov and C. Piccardi. Bifurcation analysis of periodic SEIR and SIR epidemic models. *Journal of Mathematical Biology*, 32:109–121, 1994.
- [32] A. L. Lloyd and L. Sattenspiel. Spatiotemporal dynamics of measles: synchrony and persistence in a disease metapopulation. In *Spatial Ecology*, pages 251–272. CRC Press, New York, 2009.
- [33] W. P. London and J. A. Yorke. Recurrent outbreaks of measles, chicken-pox and mumps: The role of seasonality. *American Journal of Epidemiology*, 98:453–468, 1973.
- [34] A. J. McKane and T. J. Newman. Predator-prey cycles from resonant amplification of demographic stochasticity. *Physical Review Letters*, 94:218102, 2005.
- [35] C. J. E. Metcalf, P. Klepac, M. Ferrari, N. Bharti, O. N. Bjørnstad, and B. T. Grenfell. The epidemiology of rubella in Mexico: seasonality, stochasticity and regional variation. *Epidemiology and Infection*, 139:1029–1038, 2011.
- [36] C. J. E. Metcalf, J. Lessler, P. Klepac, F. T. Cutts, and B. T. Grenfell. Minimum levels of coverage needed for rubella vaccination: impact of local demography, seasonality and population heterogeneity. *Epidemiology and Infection*, 16:1–12, 2012.
- [37] C. J. E. Metcalf, C. V. Munayco, G. Chowell, B. T. Grenfell, and O. N. Bjørnstad. Rubella meta-population dynamics and importance of spatial coupling to the risk of congenital rubella syndrome in Peru. *Journal of the Royal Society Interface*, 8:369–376, 2011.
- [38] I. Näsell. On the time to extinction in recurrent epidemics. *Journal of the Royal Statistical Society, Series B*, 61:309–330, 1997.
- [39] I. Näsell. A new look at the critical community size for childhood infections. *Theoretical Population Biology*, 67:203–216, 2005.
- [40] H. T. H. Nguyen and P. Rohani. Noise, nonlinearity and seasonality: the epidemics of whooping cough revisited. *Journal of the Royal Society Interface*, 5:403–413, 2008.
- [41] M. B. Priestley. *Spectral analysis and time series*. Academic Press, London, 1981.
- [42] H. Risken. *The Fokker-Planck Equation*. Springer, Berlin, 1996.

- [43] P. Rohani, J. D. D. Earn, and B. T. Grenfell. Opposite patterns of synchrony in sympatric disease metapopulations. *Science*, 286:968–971, 1999.
- [44] G. Rozhnova and A. Nunes. Stochastic effects in a seasonally forced epidemic model. *Physical Review E*, 82:041906, 2010.
- [45] G. Rozhnova and A. Nunes. Modelling the long-term dynamics of pre-vaccination pertussis. *Journal of the Royal Society Interface*, 9:2959–2970, 2012.
- [46] G. Rozhnova, A. Nunes, and A. J. McKane. Stochastic oscillations in models of epidemics on a network of cities. *Physical Review E*, 84:051919, 2011.
- [47] D. Schenzle. An age-structured model of pre- and post-vaccination measles transmission. *IMA Journal of Mathematics Applied in Medicine and Biology*, 1:169–191, 1984.
- [48] I. B. Schwartz. Multiple stable recurrent outbreaks and predictability in seasonally forced nonlinear epidemic models. *Journal of Mathematical Biology*, 21:347–361, 1985.
- [49] I. B. Schwartz and J. L. Aron. Seasonality and period-doubling bifurcations in an epidemic model. *Journal of Theoretical Biology*, 110:665–679, 1984.
- [50] M. Simões, M. M. Telo da Gama, and A. Nunes. Stochastic fluctuations in epidemics on networks. *Journal of the Royal Society Interface*, 5:555–566, 2008.
- [51] K. Terada. Rubella and congenital rubella syndrome in Japan: epidemiological problems. *Japanese Journal of Infectious Disease*, 56:81–87, 2003.
- [52] A. Uziel and L. Stone. Determinants of periodicity in seasonally driven epidemics. *Journal of Theoretical Biology*, 305:88–95, 2012.
- [53] O. G. van der Heijden, M. A. E. Conyn-van Spaendonck, A. D. Plantinga, and M. E. E. Kretzschmar. A model-based evaluation of the national immunization programme against rubella infection and congenital rubella syndrome in The Netherlands. *Epidemiology and Infection*, 121:653–671, 1998.
- [54] N. G. van Kampen. *Stochastic Processes in Physics and Chemistry*. Elsevier, Amsterdam, 1981.